PCCP

Accepted Manuscript

This is an *Accepted Manuscript*, which has been through the Royal Society of Chemistry peer review process and has been accepted for publication.

Accepted Manuscripts are published online shortly after acceptance, before technical editing, formatting and proof reading. Using this free service, authors can make their results available to the community, in citable form, before we publish the edited article. We will replace this *Accepted Manuscript* with the edited and formatted *Advance Article* as soon as it is available.

You can find more information about *Accepted Manuscripts* in the **Information for Authors**.

Please note that technical editing may introduce minor changes to the text and/or graphics, which may alter content. The journal's standard **Terms & Conditions** and the **Ethical guidelines** still apply. In no event shall the Royal Society of Chemistry be held responsible for any errors or omissions in this *Accepted Manuscript* or any consequences arising from the use of any information it contains.

Gate Modulation of Proton Transport in a Nanopore

Lanju Mei,[1,+] Li-Hsien Yeh,[2,+,*] and Shizhi Qian[1,*]

[1]Institute of Micro/Nanotechnology, Old Dominion University, Norfolk, VA 23529, USA

[2]Department of Chemical and Materials Engineering, National Yunlin University of Science

and Technology, Yunlin 64002, Taiwan

+ These authors contributed equally to this work

* Corresponding authors:

Fax: +886-5-5312071; E-mail: lhyeh@yuntech.edu.tw (Li-Hsien Yeh),

sqian@odu.edu (Shizhi Qian)

Abstract

Proton transport in confined spaces plays a crucial role in many biological processes as well as in modern technological applications, such as fuel cells. To achieve active control of proton conductance, we investigate for the first time the gate modulation of proton transport in a pH-regulated nanopore by a multi-ion model. The model takes into account surface protonation/deprotonation reactions, surface curvature, electroosmotic flow, Stern layer, and electric double layers overlap. The proposed model is validated by good agreement with the existing experimental data on nanopore conductance with and without a gate voltage. Results show that the modulation of proton transport in a nanopore depends on the concentration of the background salt and solution pH. Without background salt, the gated nanopore exhibits an interesting ambipolar conductance behavior when pH is close to the isoelectric point of the dielectric pore material, and the net ionic and proton conductance can be actively regulated with a gate voltage as low as 1 V. The higher the background salt concentration, the lower is the performance of the gate control on the proton transport.

Keywords: Nanofluidics; Ion Transport; Gated Nanopore; Charge Regulation; Field Effect Transistor

1. Introduction

There has been growing interest in studying the ion transport in confined spaces, such as nanopores and nanochannels,[1-3] owing to the tremendous potential of using these nanofluidic devices to control ion, fluid, and nanoparticle transports[4-10] as well as in the applications of energy conversion[11-13] and single molecule biosensing.[14, 15] Many experimental and theoretical results showed that the ion transport in such fluidic devices exhibits distinct characteristics that deviate apparently from bulk properties. For example, when the characteristic dimension of pores (or channels) shrinks to a length scale comparable to the Debye length, several unique transport behaviors, such as ion selectivity,[16, 17] local enrichment/depletion of ion concentrations,[18, 19] and rectification of ion transport,[20-22] begin to emerge. It has been demonstrated that these behaviors depend exquisitely on the surface charge property of nanopore (or nanochannel) wall.[12, 17, 23]

Proton transport (transport of H^+ ions) plays essential roles in life processes[24, 25] as well as in many modern technological applications, such as fuel cells[26] and electrochemical sensors,[27] to name a few. Compared with the significant number of researches on the transport of background ions (mainly focusing on, for example, K^+, Na^+, and Cl^- from background salts),[16, 28-43] little is known about the proton transport in confined spaces. Although Fan et al.[44] investigated experimentally the gated proton transport in aligned mesoporous silica thin films, and Chang et al.[45] modelled the equilibrium proton distribution in a nanochannel with a rectangular cross-section of $410 \times 405 \, \text{nm}^2$, a systematical theoretical study on proton transport in small nanopores (or nanochannels) under the condition of overlapped electric double layers (EDLs) has still not been reported. This might be due to the significant dependence of the proton transport on the surface charge property of nanopores, originating from the surface chemical reactions between the functional groups on the pore wall and protons. The highly coupled relationship between the mobility of protons,

surface charge properties, interfacial chemistry reactions, and local proton concentration on the pore wall significantly increases the complexity of the problem. Moreover, the presence of the other ionic species might play a role on the proton transport behavior in nanopores.

In this study, the proton and net ion transports of aqueous HCl solution in a pH-regulated nanopore gated by a field effect transistor (FET) with a gate electrode embedded outside the dielectric pore layer is investigated for the first time. It has been verified that the FET is capable of regulating the surface charge property of nanopore by modulating the gate voltage imposed on the gate electrode,[29, 46-51] thus attaining the active control. A simple model is developed with taking into account many practical effects of the multiple ionic species, electroosmotic flow, surface curvature, surface protonation/deprotonation reactions, Stern layer, and EDL overlap. In addition, the effects of an added background salt on the gate modulation of the proton and net ion transports in the nanopore are also explored.

2. Mathematical Model

The investigated system is depicted in Fig. 1, where an aqueous solution comprising four major ionic species, H^+, OH^-, Cl^-, and K^+, in a long nanopore of radius R_n, length L_n, and dielectric layer thickness δ_d is driven by an uniformly applied axial electric field $E_z = V / L_n$ with V being the voltage bias across the nanopore. A FET, comprising a gate electrode encircling entirely surrounding the dielectric layer of the nanopore, is used to regulate the zeta potential (ϕ_d), and the ion and fluid transport in the nanopore by controlling the gate voltage, V_G, imposed on the gate electrode. Due to axial symmetry, the cylindrical coordinates, r and z, are adopted with the origin fixed at the center of the nanopore.

The analysis of the considered problem is based on the following assumptions. (i) The nanopore length is sufficiently long (i.e., $L_n \gg R_n$) so that the effect of ion concentration

polarization[18, 19] is neglected and a uniform axial electric field is used. (ii) The thickness of

Stern layer, δ_s, is very thin, and ions and fluid inside that layer are immobile. (iii) The

viscosity, μ, and permittivity, ε_f, of fluid, and the diffusivity of the ith ionic species, D_i,

in the nanopore are position-independent, and the EOF velocity, u_z, is fully developed. (iv)

The applied electric field E_z is relatively weak compared with the equilibrium electric field

established by the charged nanopore. Therefore, it can be assumed that the equilibrium

electric potential within the nanopore will not be disturbed apparently by the applied potential

bias.[52, 53]

Based on these assumptions, the electrical potentials within the dielectric layer, Stern

layer, and liquid, φ, ψ, and ϕ, respectively, and the flow field can be described by

$$\frac{1}{r}\frac{d}{dr}\left(r\frac{d\varphi}{dr}\right)=0 \quad (R_n < r < R_n + \delta_d), \tag{1}$$

$$\frac{1}{r}\frac{d}{dr}\left(r\frac{d\psi}{dr}\right)=0 \quad (R_n - \delta_s < r < R_n), \tag{2}$$

$$\frac{1}{r}\frac{d}{dr}\left(r\frac{d\phi}{dr}\right)=-\frac{\rho_e}{\varepsilon_f} \quad (0 < r < R_n - \delta_s), \tag{3}$$

$$\mu\frac{1}{r}\frac{d}{dr}\left(r\frac{du_z}{dr}\right)-\varepsilon_f E_z\frac{1}{r}\frac{d}{dr}\left(r\frac{d\phi}{dr}\right)=0 \quad (0 < r < R_n - \delta_s). \tag{4}$$

In the above, $\rho_e = \frac{1}{\varepsilon_f}\sum_{i=1}^{4} Fz_iC_{i0}\exp\left(-\frac{z_iF\phi}{RT}\right)$ is the mobile space charge density;[54] z_i is the

valence of ionic species i; R, F, and T are the universal gas constant, Faraday constant,

and absolute fluid temperature, respectively. C_{i0}, $i=1$, 2, 3, and 4, denotes the bulk

concentration of H^+, OH^-, Cl^-, and K^+ ions, respectively. Due to the electroneutrality of

bulk solution in the reservoirs far away from the charged nanopore, eqn (3) can be further

simplified to (see the detailed derivation in the ESI)

$$\frac{1}{r}\frac{d}{dr}\left(r\frac{d\phi}{dr}\right) = \frac{RT\kappa^2}{zF}\sinh\left(\frac{zF\phi}{RT}\right),$$

(5)

where $z = z_1 = -z_2 = -z_3 = z_4$ and $\kappa^{-1} = \left(\varepsilon_f RT / 2z^2 F^2 C_{t0}\right)^{1/2}$ is the Debye length with

$C_{t0} = C_{10} + C_{40} = C_{20} + C_{30}$ being the bulk concentration of net cations (or anions). Note that

the present analysis is based on the Poisson-Boltzmann model, which has been demonstrated

to be sufficiently accurate for capturing the underlying physics of the ion transport in long

nanochannels with overlapped EDLs.[54] Moreover, the effect of surface curvature is taken into

account by considering the variations of φ, ψ, ϕ, and u_z along the radial direction (r) in

eqn (1)-(5).

The boundary conditions for eqn (1), (2), (4), and (5) are

$\varphi = V_G$ at $r = R_n + \delta_d$,

(6)

$\varphi = \psi = \psi_s$ at $r = R_n$,

(7)

$$\varepsilon_f \frac{d\psi}{dr} - \varepsilon_d \frac{d\varphi}{dr} = \sigma_s \text{ at } r = R_n,$$

(8)

$\psi = \phi = \phi_d$ at $r = R_n - \delta_s$,

(9)

$$\frac{d\phi}{dr} = \frac{d\psi}{dr} \text{ at } r = R_n - \delta_s,$$

(10)

$u_z = 0$ at $r = R_n - \delta_s$,

(11)

$$\frac{d\phi}{dr} = 0 \text{ at } r = 0,$$

(12)

$$\frac{du_z}{dr} = 0 \text{ at } r = 0.$$

(13)

Here, ψ_s and σ_s are the surface potential and the surface charge density of the nanopore,

respectively. Equation 12 implies that the effect of EDLs overlapping is taken into account in

the present study since we did not assume the potential at the center of the nanopore to be

zero, which was the assumption made generally in previous similar studies.[40, 41, 48]

6

The fully developed EOF velocity, u_z, can be obtained exactly by solving eqn (4) subject to eqn (11) and (13),

$$u_z = \frac{\varepsilon_f V}{\mu L}(\phi - \phi_d).$$
(14)

Solving eqn (1) and (2) subject to eqn (6), (7), and (9), we obtain

$$\varphi = \frac{(V_G - \psi_s)}{\ln(R_n + \delta_d) - \ln(R_n)}\left[\ln(r) - \ln(R_n)\right] + \psi_s,$$
(15)

$$\psi = \frac{(\psi_s - \phi_d)}{\ln(R_n) - \ln(R_n - \delta_s)}\left[\ln(r) - \ln(R_n)\right] + \psi_s.$$
(16)

From eqn (16), we obtain the difference between ψ_s and ϕ_d, which can be described by the basic Stern layer model by letting the surface capacitance of the Stern layer $C_s = \varepsilon_f / \delta_s$ [55],

$$\left.\frac{d\psi}{dr}\right|_{r=R_n} = \frac{(\psi_s - \phi_d)}{R_n \ln\left(\dfrac{R_n}{R_n - \delta_s}\right)} \approx \frac{(\psi_s - \phi_d)}{\delta_s} = \frac{C_s(\psi_s - \phi_d)}{\varepsilon_f}.$$
(17)

Suppose that the wall of dielectric nanopores in contact with aqueous solution is charge regulated due to the following two surface equilibrium chemistry reactions, $MOH \leftrightarrow MO^- + H^+$ and $MOH + H^+ \leftrightarrow MOH_2^+$. If we let K_a and K_b are the equilibrium constants of these two reactions, σ_s in eqn (8) can be described by[23]

$$\sigma_s = -\left(10^{18} \times e\Gamma_t\right)\left\{\frac{10^{-pK_a} - 10^{-pK_b}\left[C_{10} \times 10^{-3} \exp\left(-\dfrac{F\psi_s}{RT}\right)\right]^2}{10^{-pK_a} + \left[C_{10} \times 10^{-3} \exp\left(-\dfrac{F\psi_s}{RT}\right)\right] + 10^{-pK_b}\left[C_{10} \times 10^{-3} \exp\left(-\dfrac{F\psi_s}{RT}\right)\right]^2}\right\}.$$
(18)

Here, $pK_x = -\log K_x$ ($x = a$ and b); e is the elementary charge; Γ_t (in the unit of sites/nm^2) is the total site density of functional groups on the dielectric nanopore wall.

Because the thickness of the Stern layer is very thin, substituting eqn (16) into eqn (10) gives

$$\frac{d\phi}{dr}\bigg|_{r=R_n-\delta_s} = \frac{d\psi}{dr}\bigg|_{r=R_n-\delta_s} = \left[\frac{(\psi_s - \phi_d)}{\ln(R_n) - \ln(R_n - \delta_s)}\right]\left(\frac{1}{R_n - \delta_s}\right)$$

$$\approx \left[\frac{(\psi_s - \phi_d)}{\ln(R_n) - \ln(R_n - \delta_s)}\right]\left(\frac{1}{R_n}\right) = \frac{d\psi}{dr}\bigg|_{r=R_n}. \tag{19}$$

Submitting eqn (15), (18), and (19) into eqn (8), we obtain

$$\frac{d\phi}{dr}\bigg|_{r=R_n-\delta_s} = \left(\frac{\varepsilon_d}{\varepsilon_f R_n}\right)\left[\frac{(V_G - \psi_s)}{\ln(R_n + \delta_d) - \ln(R_n)}\right]$$

$$-\left(\frac{10^{18} \times e\Gamma_t}{\varepsilon_f}\right)\left\{\frac{10^{-pK_a} - 10^{-pK_b}\left[C_{10} \times 10^{-3}\exp\left(-\frac{F\psi_s}{RT}\right)\right]^2}{10^{-pK_a} + \left[C_{10} \times 10^{-3}\exp\left(-\frac{F\psi_s}{RT}\right)\right] + 10^{-pK_b}\left[C_{10} \times 10^{-3}\exp\left(-\frac{F\psi_s}{RT}\right)\right]^2}\right\}, \tag{20}$$

where ψ_s, based on eqn (17) and (19), can be replaced by

$$\psi_s = \frac{\varepsilon_f}{C_s}\frac{d\psi}{dr}\bigg|_{r=R_n} + \phi_d = \frac{\varepsilon_f}{C_s}\frac{d\phi}{dr}\bigg|_{r=R_n-\delta_s} + \phi_d. \tag{21}$$

For given conditions (pK_a, pK_b, Γ_t, C_s, V_G, δ_d, L_n, R_n, and C_{i0}, $i = 1$, 2, 3, and 4), the distributions of ϕ, and $d\phi/dr$ within the liquid phase ($0 \le r \le R_n - \delta_s$) can be easily obtained by solving eqn (5) subject to eqn (12) and (20) using, for example, the Matlab function BVP5c.

Once ϕ, and $d\phi/dr$ are determined, u_z, ϕ_d, ψ_s, and σ_s can be evaluated by eqn (14), (9), (21), and (18), respectively. Then the net ionic conductance, G (contributed from the transport of all ions),[56] can be calculated by

$$G = \frac{I}{V} = \frac{1}{V}\int_0^{R_n-\delta_s}\left[\left(\sum_{i=1}^4 Fz_i N_i\right)2\pi r\right]dr$$

$$= \left(\frac{2\pi F^2}{RTL_n}\right)\left\{\begin{array}{l}(D_1 C_{10} + D_4 C_{40})\int_0^{R_n-\delta_s}\left[\exp\left(-\frac{F\phi}{RT}\right)r\right]dr \\ + (D_2 C_{20} + D_3 C_{30})\int_0^{R_n-\delta_s}\left[\exp\left(\frac{F\phi}{RT}\right)r\right]dr\end{array}\right\} + \left(\frac{2\pi\varepsilon_f^2}{\mu L_n}\right)\left\{\int_0^{R_n-\delta_s}\left[\left(\frac{d\phi}{dr}\right)^2 r\right]dr\right\}, \tag{22}$$

8

where $N_i = \dfrac{FE_z}{RT} z_i D_i C_i + u_z C_i$ is the ionic flux of ionic species i in the z-direction in the

absence of axial concentration gradient.[57] To investigate the proton transport in the nanopore,

we further define the proton conductance, G_p (contributed only from the transport of

protons), as

$$G_p = \left(\frac{2\pi D_1 C_{10} F^2}{RT L_n} \right) \int_0^{R_n - \delta_s} \left[\exp\left(-\frac{F\phi}{RT} \right) r \right] dr + \left(\frac{2\pi \varepsilon_f F C_{10}}{\mu L_n} \right) \int_0^{R_n - \delta_s} \left[\exp\left(-\frac{F\phi}{RT} \right) (\phi - \phi_d) r \right] dr \quad (23)$$

3. Results and Discussion

In typical experiments, the pH of a electrolyte solution can be adjusted by adding an acid,

HCl, or a base, KOH, and its ionic strength can be determined by a background salt, KCl, of

concentration C_{salt}. In the present study, we focus on the proton transport in a nanopore and,

therefore, the solution pH is limited at an acidic environment. If $pH < 7$, electroneutrality of

the bulk solution yields $C_{10} = 10^{-pH+3}$, $C_{20} = 10^{-(14-pH)+3}$, $C_{30} = C_{salt} + 10^{-pH+3} - 10^{-(14-pH)+3}$,

and $C_{40} = C_{salt}$.[58] In subsequent sections, in addition to the model validation by the

experimental data available from the literature, the influences of pH and the gate voltage, V_G,

on the gate modulation of proton transport in a nanopore in the absence ($C_{salt} = 0$) and

presence ($C_{salt} \neq 0$) of a background salt (KCl) are thoroughly discussed. At $T = 298$ K, the

ionic diffusivities of H^+ (D_1), OH^- (D_2), Cl^- (D_3), and K^+ (D_4) are fixed at 9.31,

5.30, 2.03, and 1.96 ($\times 10^{-9}$ m^2/s), respectively.[59]

3.1. Model Validation by Experimental Data

The model verification is conducted by fitting its prediction to the experimental data of

Joshi et al.[60], where the FET modulation of the net ionic conductance (G) of an array of 25

cylindrical nanopores in an aqueous HCl solution (i.e., $C_{salt} = 0$) for the cases of both active

($V_G = 0.3$ V) and inactive ($V_G = 0$ V) FET was performed. The geometry of the cylindrical

nanofluidic FET is $R_n = 17$ nm, $L_n = 340$ nm, and $\delta_d = 60$ nm. Fig. 2 shows the variations

of modulated G and surface charge density σ_s as a function of the molar concentration of

protons, $[H^+]_0 = 10^{-pH}$, in the range of $10^{-6} \sim 10^{-2}$ M (corresponding to pH from 6 to 2). As

depicted in Fig. 2a, for both active and inactive FET, the results predicted from the present

model at $pK_a = 7.7$, $pK_b = 0$, $\Gamma_t = 8$ sites/nm^2, and $C_s = 0.15$ F/m^2 (lines) are in good

agreement with the experimental data of Joshi et al.[60] (symbols). Note that especially in the

low regime of $[H^+]_0$ (or high regime of pH), in which the EDLs are overlapped, the

nanopore conductance slowly and nonlinearly decreases with decreasing $[H^+]_0$, which can

be excellently described by the present model. The nonlinear dependence of G on $[H^+]_0$

at low proton concentration shows the typical nanopore conductance behavior.[1, 28, 44] This is

because under the condition of overlapped EDLs, the nanopore conductance becomes

governed by the surface charge of nanopore.[28] Because the negative σ_s increases slightly

with decreasing $[H^+]_0$ (Fig. 2b), the slight decrease of G with decreasing $[H^+]_0$ at low

$[H^+]_0$ (Fig. 2a) is primarily dominated by the decreasing proton concentration. Note that

H^+ ions are the sole counterions for the system under consideration.

As demonstrated in Fig. 2, our model taking into account the EDL overlap, interfacial

chemistry reactions on the pore wall, and the presence of H^+ and OH^- ions, is capable of

capturing the underlying physics of the gate control of ion transport in a nanopore. Therefore,

the developed model along with the above fitted parameters of pK_a, pK_b, Γ_t, and C_s is

then used in the following investigations on the gate modulation of proton transport in a

nanopore. For illustration, we fix the geometry of the gated nanopore at $R_n = 5$ nm,

$L_n = 1$ μm, and $\delta_d = 40$ nm.

3.2. Gate Modulation of Proton Transport

Fig. 3 depicts the influence of pH on the gate modulation of the net ionic conductance G, proton conductance G_p, relative percentage of G_p/G, and enhanced ratio of protons, α_H, in the nanopore without a background salt ($C_{salt} = 0$), which implies that only three kinds of ionic species, H^+, OH^-, and Cl^-, are considered at $pH < 7$. We define α_H as

$$\alpha_H = \frac{\int_0^{R_n - \delta_s} (C_1 2\pi r)\, dr}{C_{10} \pi R_n^2} \approx \frac{\int_0^{R_n} (C_1 2\pi r)\, dr}{C_{10} \pi R_n^2}, \tag{24}$$

where $C_1 = C_{10} \exp(-F\phi/RT)$. If $\alpha_H > 1$ (<1), the more significant deviation of α_H from 1 indicates the more significant enhancement (depletion) of protons by the gated nanopore. Fig. 3a shows that the gate modulation of G depends on the levels of pH. For example, the modulated G is nearly independent of the gate voltage at extremely low pH (e.g., 1), has a local minimum as V_G varies at moderately low pH (e.g., 2 and 4), and decreases monotonically with V_G ranging from -15 to 15 V when pH is further increased (e.g., 6). However, Fig. 3b shows that G_p, regardless of the levels of pH, decreases monotonically with the variation of V_G from -15 to 15 V. Fig. 3c shows that G_p/G is nearly 100% for $pH = 4$ and 6 with negative V_G. However, for $V_G > 0$, the ratio G_p/G gradually decreases for $pH = 6$ and becomes nearly 0 for $pH = 4$ as the positive V_G increases. For $pH = 1$ and 2, the ratio G_p/G monotonically decreases as V_G increases from -15 to 15 V. Fig. 3d shows that protons inside the nanopore are slightly depleted for $pH = 1$, and are enriched (depleted) for negative (positive) V_G at $pH = 2$ and 4. For $pH = 6$, protons are significantly enriched when V_G is smaller than a critical value, beyond which protons are depleted. Clearly, the modulation of the proton conductance by the gate potential depends on the solution pH.

If pH is extremely low (e.g., $\mathrm{pH}=1$ and the corresponding $\kappa R_n = 5.20$), the dependence of G on the gate voltage at extremely high proton concentration can be attributed to the bulk conductance behavior,[44, 60] implying that the behavior of G is nearly independent of the surface charge property (e.g., zeta potential, ϕ_d) of a nanopore modulated by V_G shown in Fig. S1 of the ESI. At $\mathrm{pH}=1$ the nanopore is positively charged, and its zeta potential increases as V_G increases from -15 to 15 V, as shown in Fig. S1. Thus protons are depleted from the positively charged nanopore. However, since the corresponding EDL is very thin, the cross-section averaged proton concentration is only slightly below its bulk value, yielding α_H slightly below 1 as shown in Fig. 3d. Mainly due to the thin EDL, the net ionic conductance, G, is carried by the ions in the bulk region of the nanopore, which is independent of the gate voltage, as shown in Fig. 3a. As V_G increases, more protons are depleted, resulting in a decrease in α_H, G_p, and G_p/G as shown in Fig. 3. For example, G_p/G reduces from about 80% at $V_G = -15\,\mathrm{V}$ to about 51% at $V_G = 15\,\mathrm{V}$. Although the nanopore is positively charged, since the diffusivity of protons is much higher than those of anions, the ratio of G_p/G is still larger than 50% as shown in Fig. 3c, implying that the net ionic conductance in the nanopore is dominated primarily by the proton conductance, and the ionic flux of protons dominates over that of other anions.

As pH increases, the ionic concentration decreases and the degree of EDL overlapping increases. The dependence of G on V_G is due to the emergence of the surface charge-governed phenomenon[28] and can be explained by the gate modulation of the zeta potential (ϕ_d) shown in Fig. S1 of the ESI. For example, the behavior that G decreases with V_G at $\mathrm{pH}=2$ and 4 seen in Fig. 3a can be attributed to the decrease of the negative ϕ_d (Fig. S1). On the other hand, the increase of G with increasing positive V_G arises from the

increase of the positive ϕ_d (Fig. S1), which reduces the transport of protons (coions) but

enhances the transport of OH^- and Cl^- (counterions). Note that the interesting ambipolar

behavior of G with V_G[61] only occurs when pH is close to the isoelectric point (IEP) of

considered dielectric pore material ($(pK_a - pK_b)/2 = 3.85$), which makes its zeta potential

much easier to be tuned from negative to positive by gate voltage,[36] as shown in Fig. S1. This

explains why G shows a local minimum with V_G at pH $= 2$ and 4, as shown in Fig. 3a.

In the range of V_G with a negative surface charge, the trend of G_p with V_G is the same as

that of G. However, in the range of V_G with a positive charge, due to more significant

depletion of protons with an increase in the positive ϕ_d tuned by a positive V_G, the proton

conductance decreases as V_G increases, as shown in Fig. 3b. At pH $= 4$ (the corresponding

$\kappa R_n = 0.16$), protons are significantly enriched (depleted) with negative (positive) V_G, and

the concentration of protons exhibits a sharp variation with V_G ranging from -1 and 1 V,

as shown in Fig. 3d. In addition, the diffusivity of protons is much higher than those of OH^-

and Cl^-. These two factors result in $G_p / G \approx 100\%$ for negative V_G and 0 for positive

V_G. The change of G_p / G with V_G for pH $= 2$ (the corresponding $\kappa R_n = 1.64$) is also

due to the modulation of surface charge and proton concentration by V_G. However, since the

EDL at pH $= 2$ is not overlapped, the concentration of protons only gradually decreases

with V_G, as shown in Fig. 3d. Thus variation of G_p / G with V_G for pH $= 2$ is not as

significant as that for pH $= 4$. Results clearly show that the transport of protons can be

actively modulated by the FET with a gate voltage as low as 1 V when pH is close to the IEP

of the nanopore, which is different from the reported experimental results in the presence of a

background salt,[29, 46, 62] in which a higher gate voltage (typically on the order of ten volts) is

required and a modest variation can be realized.

At $pH = 6$ (the corresponding $\kappa R_n = 0.02$), the nanopore wall remains negatively charged and the magnitude of the negative zeta potential decreases as V_G increases from -15 to 8 V. Due to the EDL overlap and the surface charge-governed ion transport, both the net ion conductance (G) and the proton conductance (G_p) decrease monotonically as V_G varies from -15 to 8 V, as shown in Fig. 3a and 3b. The nanopore becomes slightly positively charged when V_G exceeds 8 V, and further increase in V_G results in a decrease in proton concentration, yielding the decrease in both G and G_p. The significantly enriched proton concentration yields $G_p / G \approx 100\%$ for negative V_G. For positive V_G, G_p / G gradually decreases with V_G, which is attributed to the decrease in the proton concentration, as shown in Fig. 3d.

We further investigate the influence of the molar concentration of protons, $[H^+]_0$, on the net ionic conductance G, proton conductance G_p, relative percentage of G_p / G, and enhanced ratio of protons, α_H, for various gate voltages V_G, as depicted in Fig. 4. Fig. 4a and b reveals that both G and G_p decrease linearly with decreasing $[H^+]_0$ for higher $[H^+]_0$ and gradually plateau with a further decrease in $[H^+]_0$ for relatively lower $[H^+]_0$. Moreover, both G and G_p are independent of V_G when $[H^+]_0$ is sufficiently high, exhibiting a bulk conductance behavior, and vary remarkably with V_G when $[H^+]_0$ is relatively low, exhibiting the expected surface charge-governed conductance behavior.

Fig. 4c indicates that if $[H^+]_0$ is sufficiently low, G_p / G at any level of V_G approaches unity, implying that the behavior of G is dominated approximately entirely by that of G_p. This can be explained by Fig. 4d, in which the proton concentration in the nanopore is remarkably enhanced as a result of the significant EDL overlapping effect and

high negative zeta potential (see Fig. S2 of the ESI). Therefore, the proton transport behavior

dominates absolutely the net ion transport behavior in the nanopore. As $[H^+]_0$ increases,

G_p / G, regardless of the level of V_G, first decreases, attains a minimum, and then increases.

The decrease of G_p / G with $[H^+]_0$ can be attributed to the decrease in the degree of EDL

overlapping and the magnitude of the negative zeta potential with an increase in $[H^+]_0$ (Fig.

S2), both of which yield a decrease in the proton concentration inside the nanopore (Fig. 4d).

The increase of G_p / G with $[H^+]_0$ is due to the decrease in the degree of EDL overlapping

and an increase in the bulk concentration of protons inside the nanopore. If $[H^+]_0$ is

extremely high (e.g., $\kappa R_n \quad 1)$, the nanopore is filled with abundant protons like its bulk

state (Fig. 4d) and its zeta potential is very small (Fig. S2). Therefore, the gate voltage has

negligible effect on the variation of G_p / G, implying that the net ionic conductance in the

nanopore contributes mainly from its proton conductance no matter if the FET is active or

not.

3.3. Influence of Background Salt on the Gate Modulation of Proton Transport

Fig. 5 summarizes the influence of the concentration of background salt C_{salt} on the gate

modulation of the net ionic conductance G, proton conductance G_p, relative percentage of

G_p / G, and enhanced ratio of protons, α_H, at $pH = 3.5$. Note that the choice of $pH = 3.5$

is due to better performance of gate control when the solution pH is close to the IEP of the

dielectric pore material as mentioned previously. As seen in Fig. 5a, if C_{salt} is relatively

high (e.g., 100 mM), G is nearly independent of the gate voltage V_G (bulk conductance

behavior); however, if C_{salt} is relatively low, G shows a local minimum as V_G varies

(ambipolar conductance behavior), which is similar to the results shown in Fig. 3a ($pH = 2$

and 4) and can be explained by the same reasoning of bipolar charge properties at different

polarities of V_G. Fig. 5a also indicates the performance of the gate modulation of G decreases with an increase in C_{salt}. This is due to the decrease in the EDL thickness, yielding more counterions confined near the nanopore surface. Under this condition, the FET is harder to effectively tune the zeta potential of the nanopore (see Fig. S3 of the ESI) and, therefore, the nanopore conductance.

Fig. 5b shows that the proton conductance, G_p, decreases monotonically with the gate voltage, V_G, varying from -15 to 15 V, which is inconsistent with the gate modulation of the net ionic conductance, G, depicted in Fig. 5a. If $V_G < 0$, the decrease of G_p is due to the decrease in both the magnitude of negative ϕ_d (Fig. S3) and the proton concentration (Fig. 5d). When $V_G > 0$, a further decrease of G_p with increasing V_G arises from the more significant exclusion of protons with increasing positive ϕ_d (Fig. S3). Apparently, Fig. 5b indicates that the performance of the gate modulation of proton conductance in the nanopore becomes less significant as the added background salt concentration increases, which is in accordance with the result of G shown in Fig. 5a.

Fig. 5c shows that if $V_G < 0$, the proton conductance, G_p, plays a dominate role on the net ionic conductance, G, for relatively low background salt concentration, C_{salt}, and the contribution of G_p to G decreases with an increase in C_{salt}. The former arises from the significant enhancement of protons (see Fig. 5d) by the modulated negatively charged nanopore. The latter can be attributed to the excluded effect of protons by the other increased amount of counterions, K^+, dissociated from the background salt.[23] On the other hand, if $V_G > 0$, since the nanopore becomes positively charged (see Fig. S3), Fig. 5c reveals that the proton conductance, regardless of the background salt concentration, plays negligible role on the net ionic conductance ($G_p / G \rightarrow 0$), implying that the nanopore conductance is

dominated majorly by anions (n-type transistor). Consequently, the proton concentration in

the nanopore is down off below its bulk value (pink region), as shown in Fig. 5d. Because the

magnitude of the zeta potential decreases as C_{salt} increases (see Fig. S3), Fig. 5d reveals that

the enhanced (or reduced) effect of protons for $V_G < 0$ ($V_G > 0$) decreases accordingly.

To further investigate the background salt effect, the dependence of G, G_p, G_p/G,

and α_H on C_{salt} for various levels of V_G at $pH = 3.5$ are shown in Fig. 6. As expected,

Fig. 6a reveals that if C_{salt} is sufficiently high, the nanopore exhibits a bulk conductance

behavior and G is independent of V_G. However, if C_{salt} is low, the

surface-charge-governed conductance behavior emerges and G becomes highly dependent

on V_G. Similar phenomena can also be found in the gate modulation of G_p shown in Fig.

6b, suggesting that the lower the background salt concentration, the more significant the gate

modulation of ion and proton transports. It should be noted in Fig. 6b that for inactive FET

($V_G = 0$ V), the proton conductance increases with increasing C_{salt}, while decreases with

increasing C_{salt} for active FET with a negative gate voltage ($V_G < 0$). These behaviors can

be explained by the gate modulation of ϕ_d as depicted in Fig. S4 of the ESI. Because the

considered solution pH is lower than the IEP (e.g., 3.85) of dielectric pore material, the

nanopore is positively charged with $\phi_d > 0$, repelling coions, including protons, outside the

nanopore when $V_G = 0$. An increased background salt results in a decreased zeta potential of

the nanopore (Fig. S4) and, therefore, a mitigated effect of retarding proton transport. This

also explains the behavior shown in Fig. 6d that $\alpha_H < 1$ (pink region) and increases with

increasing C_{salt} for $V_G = 0$ V. Furthermore, the zeta potential (ϕ_d) of the nanopore can be

modulated from positive to negative, which attracts more protons into the nanopore and thus

yields a higher proton conductance, if a negative gate voltage ($V_G < 0$) is applied to the gate

electrode. Similarly, the negative ϕ_d decreases as C_{salt} increases (see Fig. S4), yielding a decrease of the proton conductance (Fig. 6b) and the enhanced ratio of protons (Fig. 6d) in the nanopore.

It is worth noting in Fig. 6c that if a small negative gate voltage ($-1\ \text{V} \leq V_G \leq -0.2\ \text{V}$) is applied to the gate electrode, the relative percentage of G_p / G decreases significantly from over 80 % to nearly 0 % as C_{salt} increases from 0.1 to 10 mM. This implies that protons dominantly contribute to the net ionic conductance of the nanopore for $C_{salt} < 0.1\ \text{mM}$, but contribute little when $C_{salt} > 10\ \text{mM}$. This arises from the fact that the proton concentration at $\text{pH} = 3.5$ is comparably higher than other ions for $C_{salt} < 0.1\ \text{mM}$ and the ionic mobility of H^+ is apparently larger than the other cations K^+ from background salt KCl. Because the nanopore is negatively charged when $-1\ \text{V} \leq V_G \leq -0.2\ \text{V}$, the ion transport in the nanopore is primarily dominated by the transport of major cations, H^+, if the concentration of background salt is low. Because the proton concentration is normally high at $\text{pH} = 3.5$, Fig. 6c shows that the net ionic conductance in the nanopore for sufficiently low C_{salt} is still dominated by the proton conductance (e.g., $G_p / G > 60\%$) even though the nanopore is positively charged at $V_G = 0\ \text{V}$.

4. Conclusions

In summary, a model, taking into account the effects of multiple ionic species, electroosmotic flow, surface curvature, surface protonation/deprotonation reactions, Stern layer, and electric double layers overlap, is developed to investigate the gate modulation of proton transport in a pH-Regulated nanopore. To validate the proposed model, we compare its predictions to the existing experimental data of the nanopore conductance in the absence and presence of a gate voltage, and both cases obtain good agreement. Further parametric

studies show that the gate modulation of proton transport in the nanopore depends significantly on the solution pH and the concentration of an added background salt. For example, if a background salt is absent, the ion transport behavior in the nanopore is dominated primarily by its proton transport when pH is extremely low and sufficiently high. However, when pH is close to the isoelectric point of the dielectric pore material, the modulated ion transport behavior is dominated majorly by the transport behavior of protons (the other anions) at negatively (positively) gate voltage bias, and an interesting ambipolar conductance behavior can be observed. The presence of a background salt affects significantly the gate modulation of ion and proton transports in the nanopore. Typically, the higher the background salt concentration, the lower the performance of the gate modulation behavior. It is worth noting that in the absence of a background salt both the net ionic and proton conductances can be actively controlled with a gate voltage as low as 1 V at sufficiently high pH near the IEP of the nanopore material, which has potential applications on the gated nanofluidic devices for regulating ion and biomolecular transports.

Electronic supplementary information (ESI) available: The detailed derivation of eqn (3) and (5) and the results of the gate modulation of the zeta potential of the nanopore for the case of Fig. 3-6.

References

1. R. B. Schoch, J. Y. Han and P. Renaud, *Rev. Mod. Phys.*, 2008, **80**, 839-883.

2. K. Mawatari, Y. Kazoe, H. Shimizu, Y. Pihosh and T. Kitamori, *Anal. Chem.*, 2014, **86**, 4068-4077.

3. D. G. Haywood, A. Saha-Shah, L. A. Baker and S. C. Jacobson, *Anal. Chem.*, 2015, **87**, 172-187.

4. W. J. Lan, D. A. Holden and H. S. White, *J. Am. Chem. Soc.*, 2011, **133**, 13300-13303.

5. S. F. Buchsbaum, G. Nguyen, S. Howorka and Z. S. Siwy, *J. Am. Chem. Soc.*, 2014, **136**, 9902-9905.

6. M. Schiel and Z. S. Siwy, *J. Phys. Chem. C*, 2014, **118**, 19214-19223.

7. L. Zeng, Z. Yang, H. C. Zhang, X. Hou, Y. Tian, F. Yang, J. J. Zhou, L. Li and L. Jiang, *Small*, 2014, **10**, 793-801.

8. Z. Zhang, X. Y. Kong, K. Xiao, Q. Liu, P. Li, J. Ma, Y. Tian, L. P. Wen and L. Jiang, *J. Am. Chem. Soc.*, 2015, **137**, 14765-14772.

9. Z. Zhang, X. Y. Kong, K. Xiao, G. H. Xie, Q. Liu, Y. Tian, H. Zhang, J. Ma, L. P. Wen and L. Jiang, *Adv. Mater.*, 2016, **28**, 144-150.

10. L. P. Wen, X. Hou, Y. Tian, F. Q. Nie, Y. L. Song, J. Zhai and L. Jiang, *Adv. Mater.*, 2010, **22**, 1021-1024.

11. C. Davidson and X. C. Xuan, *J. Power Sources*, 2008, **179**, 297-300.

12. A. Siria, P. Poncharal, A. L. Biance, R. Fulcrand, X. Blase, S. T. Purcell and L. Bocquet, *Nature*, 2013, **494**, 455-458.

13. J. Gao, W. Guo, D. Feng, H. T. Wang, D. Y. Zhao and L. Jiang, *J. Am. Chem. Soc.*, 2014, **136**, 12265-12272.

14. M. Tsutsui, Y. H. He, M. Furuhashi, S. Rahong, M. Taniguchi and T. Kawai, *Sci. Rep.*, 2012, **2**, 0394.

15. L. Z. Chen, H. L. He and Y. D. Jin, *Anal. Chem.*, 2015, **87**, 522-529.

16. I. Vlassiouk, S. Smirnov and Z. Siwy, *Nano Lett.*, 2008, **8**, 1978-1985.

17. Z. Zeng, L. H. Yeh, M. Zhang and S. Qian, *Nanoscale*, 2015, **7**, 17020-17029.

18. L. H. Yeh, M. Zhang, S. Qian, J. P. Hsu and S. Tseng, *J. Phys. Chem. C*, 2012, **116**, 8672-8677.

19. M. Jia and T. Kim, *Anal. Chem.*, 2014, **86**, 7360-7367.

20. Z. S. Siwy, *Adv. Funct. Mater.*, 2006, **16**, 735-746.

21. H. S. White and A. Bund, *Langmuir*, 2008, **24**, 2212-2218.

22. D. H. Lin, C. Y. Lin, S. Tseng and J. P. Hsu, *Nanoscale*, 2015, **7**, 14023-14031.

23. L. H. Yeh, M. Zhang and S. Qian, *Anal. Chem.*, 2013, **85**, 7527-7534.

24. T. Elston, H. Y. Wang and G. Oster, *Nature*, 1998, **391**, 510-513.

25. T. E. Decoursey, *Physiol. Rev.*, 2003, **83**, 475-579.

26. K. D. Kreuer, S. J. Paddison, E. Spohr and M. Schuster, *Chem. Rev.*, 2004, **104**, 4637-4678.

27. A. Heller and B. Feldman, *Chem. Rev.*, 2008, **108**, 2482-2505.

28. D. Stein, M. Kruithof and C. Dekker, *Phys. Rev. Lett.*, 2004, **93**, 035901.

29. R. Karnik, R. Fan, M. Yue, D. Y. Li, P. D. Yang and A. Majumdar, *Nano Lett.*, 2005, **5**, 943-948.

30. Y. Ai, M. K. Zhang, S. W. Joo, M. A. Cheney and S. Qian, *J. Phys. Chem. C*, 2010, **114**, 3883-3890.

31. L. H. Yeh, M. Zhang, N. Hu, S. W. Joo, S. Qian and J. P. Hsu, *Nanoscale*, 2012, **4**, 5169-5177.

32. J. R. Wang, L. Zhang, J. M. Xue and G. Q. Hu, *Biomicrofluidics*, 2014, **8**, 024118.

33. J. T. Wang, M. H. Zhang, J. Zhai and L. Jiang, *Phys. Chem. Chem. Phys.*, 2014, **16**, 23-32.

34. S. Tseng, Y. H. Tai and J. P. Hsu, *Microfluid. Nanofluid.*, 2014, **17**, 933-941.

35. Y. C. Chung, J. P. Hsu and S. Tseng, *J. Phys. Chem. C*, 2014, **118**, 19498-19504.

36. L. H. Yeh, Y. Ma, S. Xue and S. Z. Qian, *Sens. Actuator B-Chem.*, 2015, **215**, 266-271.

37. M. Taghipoor, A. Bertsch and P. Renaud, *ACS Nano*, 2015, **9**, 4563-4571.

38. M. Taghipoor, A. Bertsch and P. Renaud, *Phys. Chem. Chem. Phys.*, 2015, **17**, 4160-4167.

39. C. Y. Lin, L. H. Yeh, J. P. Hsu and S. Tseng, *Small*, 2015, **11**, 4594-4602.

40. Y. Ma, S. Xue, S. C. Hsu, L. H. Yeh, S. Qian and H. Tan, *Phys. Chem. Chem. Phys.*, 2014, **16**, 20138-20146.

41. Y. Ma, L. H. Yeh and S. Qian, *Electrochem. Commun.*, 2014, **43**, 91-94.

42. W. H. Guan, R. Fan and M. A. Reed, *Nat. Commun.*, 2011, **2**, 506.

43. S. J. Tseng, C. H. Chang, J. P. Hsu and B. T. Liu, *Electrochem. Commun.*, 2014, **48**, 169-172.

44. R. Fan, S. Huh, R. Yan, J. Arnold and P. D. Yang, *Nat. Mater.*, 2008, **7**, 303-307.

45. C. C. Chang, Y. Kazoe, K. Morikawa, K. Mawatari, R. J. Yang and T. Kitamori, *Anal. Chem.*, 2013, **85**, 4468-4474.

46. R. Fan, M. Yue, R. Karnik, A. Majumdar and P. D. Yang, *Phys. Rev. Lett.*, 2005, **95**, 086607.

47. L. H. Yeh, S. Xue, S. W. Joo, S. Qian and J. P. Hsu, *J. Phys. Chem. C*, 2012, **116**, 4209-4216.

48. C. Hughes, L. H. Yeh and S. Qian, *J. Phys. Chem. C*, 2013, **117**, 9322-9331.

49. W. H. Guan, S. X. Li and M. A. Reed, *Nanotechnology*, 2014, **25**, 122001.

50. Y. H. He, M. Tsutsui, C. Fan, M. Taniguchi and T. Kawai, *ACS Nano*, 2011, **5**, 5509-5518.

51. Y. H. He, M. Tsutsui, C. Fan, M. Taniguchi and T. Kawai, *ACS Nano*, 2011, **5**, 8391-8397.

52. A. Revil, *J. Colloid Interface Sci.*, 1999, **212**, 503-522.

53. B. T. Liu, S. Tseng and J. P. Hsu, *Electrochem. Commun.*, 2015, **54**, 1-5.

54. Y. Ma, L. H. Yeh, C. Y. Lin, L. J. Mei and S. Z. Qian, *Anal. Chem.*, 2015, **87**, 4508-4514.

55. S. H. Behrens and D. G. Grier, *J. Chem. Phys.*, 2001, **115**, 6716-6721.

56. M. J. Huang, L. J. Mei, L. H. Yeh and S. Z. Qian, *Electrochem. Commun.*, 2015, **55**, 60-63.

57. L. H. Yeh, C. Hughes, Z. Zeng and S. Qian, *Anal. Chem.*, 2014, **86**, 2681-2686.

58. Z. Milne, L. H. Yeh, T. H. Chou and S. Qian, *J. Phys. Chem. C*, 2014, **118**, 19806-19813.

59. L. H. Yeh, Y. Ma, S. Xue and S. Qian, *Electrochem. Commun.*, 2014, **48**, 77-80.

60. P. Joshi, A. Smolyanitsky, L. Petrossian, M. Goryll, M. Saraniti and T. J. Thornton, *J. Appl. Phys.*, 2010, **107**, 054701.

61. S. H. Lee, H. Lee, T. Jin, S. Park, B. J. Yoon, G. Y. Sung, K. B. Kim and S. J. Kim, *Nanoscale*, 2015, **7**, 936-946.

62. U. Vermesh, J. W. Choi, O. Vermesh, R. Fan, J. Nagarah and J. R. Heath, *Nano Lett.*, 2009, **9**, 1315-1319.
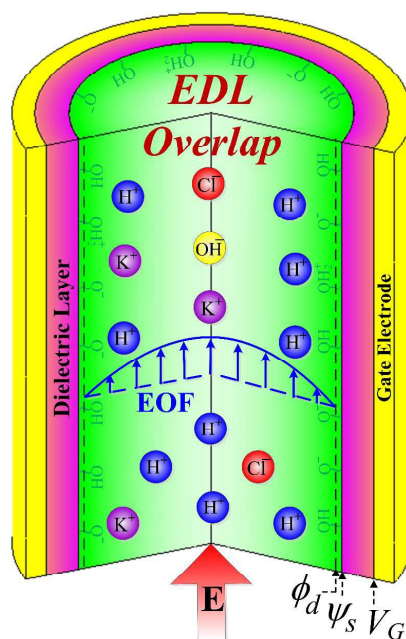
List of Figures

Fig. 1. Schematic of the gate control of ion and fluid transport in a long, pH-regulated, cylindrical nanopore filled with an aqueous solution comprising multiple ionic species, H^+, OH^-, Cl^-, and K^+. V_G is the gate voltage applied to the gate electrode, which can be used to regulate the surface potential (ψ_s) and zeta potential (ϕ_d) of the nanopore.
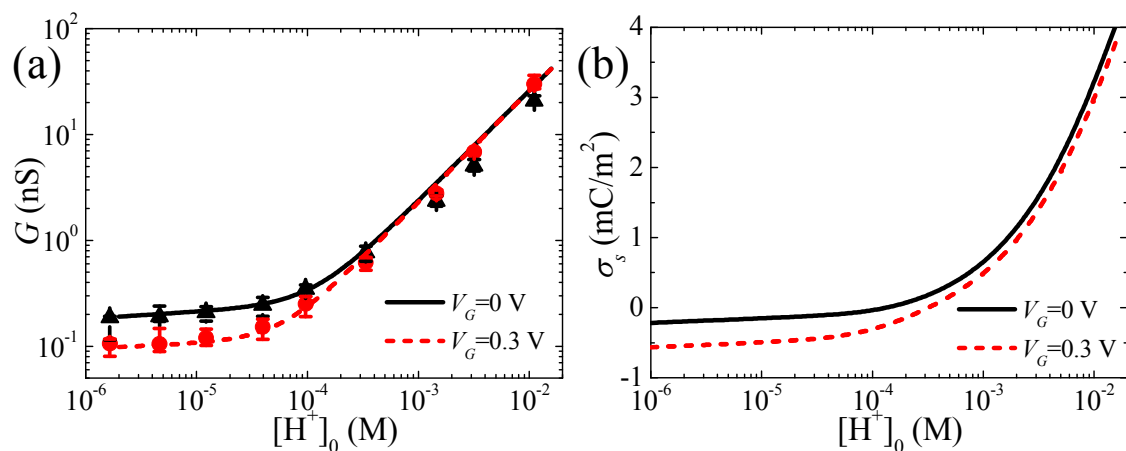
Fig. 2. Gate modulation of the nanopore conductance G, (a), and surface charge density σ_s, (b), as a function of the molar concentration of protons, $[H^+]_0$, adjusted by the background HCl solution. Triangles and spheres in (a) denote, respectively, the experimental data of Joshi et al.[60] for an inactive ($V_G = 0$ V) and active ($V_G = 0.3$ V) FET at $R_n = 17$ nm, $L_n = 340$ nm, and $\delta_d = 60$ nm. Lines denote the present results at $pK_a = 7.7$, $pK_b = 0$, $\Gamma_t = 8$ sites/nm^2, and $C_s = 0.15$ F/m^2.
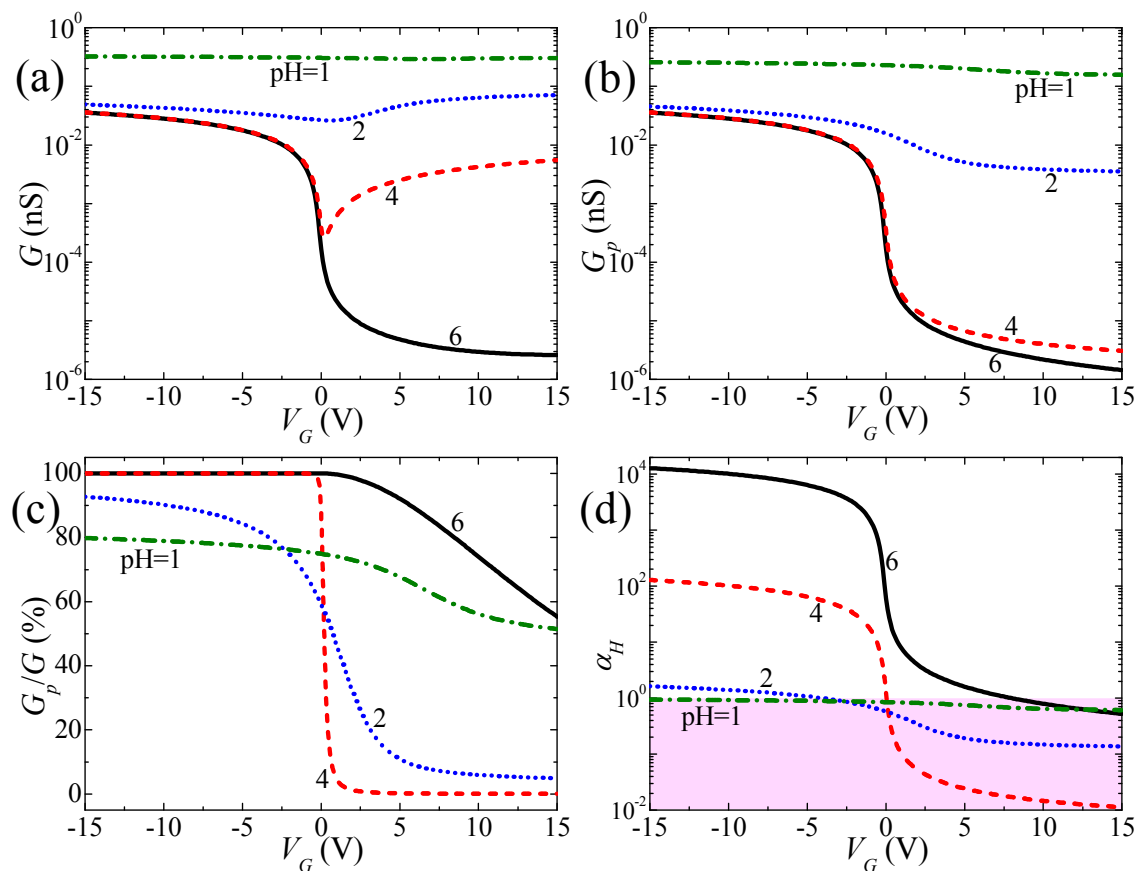
Fig. 3. Gate modulation of the net ionic conductance G, (a), proton conductance G_p, (b), relative percentage of G_p / G, (c), and enhanced ratio of protons, $\alpha_H = \bar{C}_1 / C_{10}$, as a function of V_G for various pHs without background salt ($C_{salt} = 0$ mM). The pink region in (d) highlights where the proton concentration inside the nanopore is depressed ($\alpha_H < 1$).
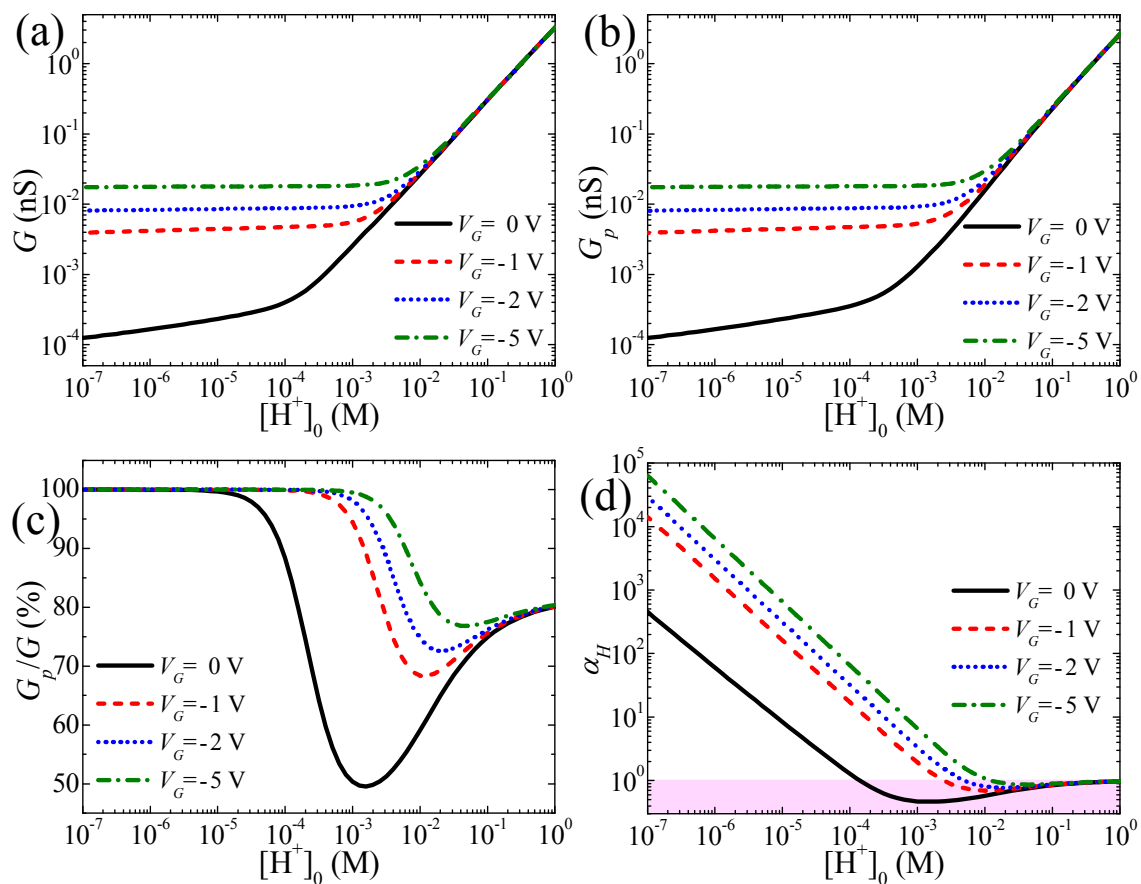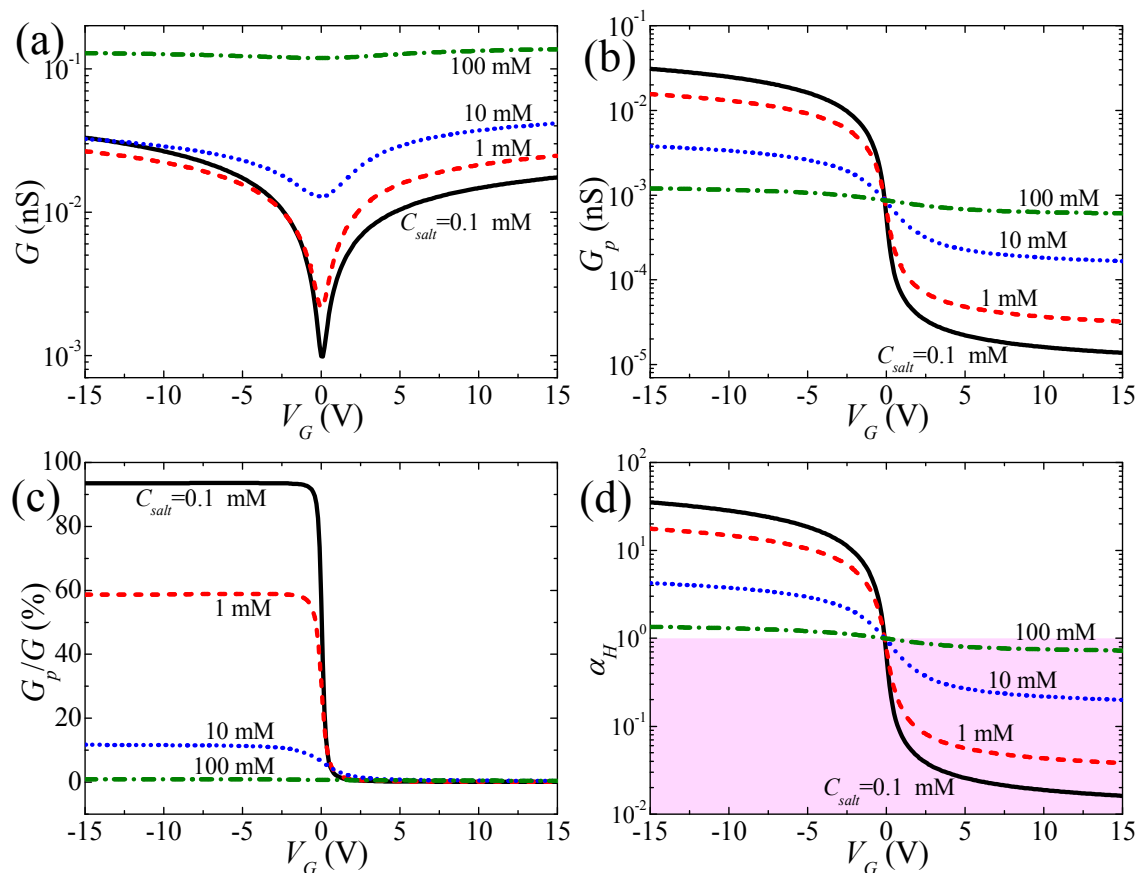
Fig. 4. Gate modulation of the net ionic conductance G, (a), proton conductance G_p, (b), relative percentage of G_p / G, (c), and enhanced ratio of protons, $\alpha_H = \overline{C}_1 / C_{10}$, as a function of the molar concentration of protons, $[H^+]_0$, for various levels of V_G without background salt ($C_{salt} = 0\ \text{mM}$). The pink region in (d) highlights where the proton concentration inside the nanopore is depressed ($\alpha_H < 1$).

Fig. 5. Gate modulation of the net ionic conductance G, (a), proton conductance G_p, (b), relative percentage of G_p / G, (c), and enhanced ratio of protons, $\alpha_H = \bar{C}_1 / C_{10}$, as a function of V_G for various background salt concentrations C_{salt} at $\mathrm{pH} = 3.5$. The pink region in (d) highlights where the proton concentration inside the nanopore is depressed ($\alpha_H < 1$).
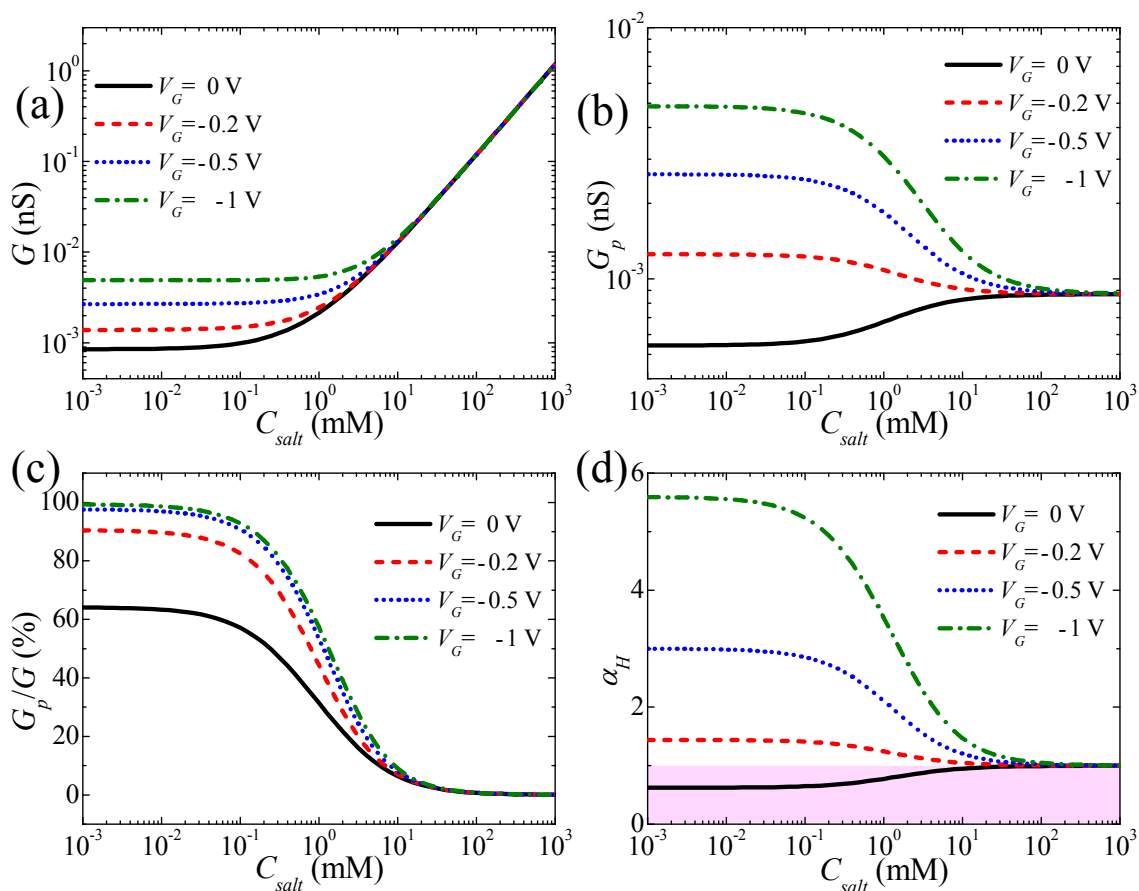
Fig. 6. Gate modulation of the net ionic conductance G, (a), proton conductance G_p, (b), relative percentage of G_p/G, (c), and enhanced ratio of protons, $\alpha_H = \bar{C}_1 / C_{10}$, as a function of the background salt concentration C_{salt} for various levels of V_G at pH $= 3.5$. The pink region in (d) highlights where the proton concentration inside the nanopore is depressed ($\alpha_H < 1$).